

Occurrence of solid noble-gas inclusions in ion-beam-implanted magnesium oxide

M. Grant Norton, Elizabeth L. Fleischer, William Hertl, C. Barry Carter, and James W. Mayer
Department of Materials Science and Engineering, Cornell University, Ithaca, New York 14853

Eric Johnson

Physics Laboratory, H.C. Ørsted Institute, DK-2100, Copenhagen Ø, Denmark

(Received 17 October 1990)

Ion implantation of xenon into single-crystal magnesium oxide results in the formation of solid, crystalline xenon inclusions. These inclusions have been investigated by transmission electron microscopy and selected-area diffraction. The solid inclusions could be divided into two categories: those that were epitactically aligned with the matrix and those that were randomly oriented. The formation of solid inclusions at room temperature indicates that they were under a high pressure. This pressure was calculated to be ~ 0.4 – 0.6 GPa.

The formation of solid noble-gas inclusions following ion implantation is not a new discovery. In 1984 it was found that noble-gas atoms implanted into metals could be trapped in a solid form.^{1,2} A number of further observations on the nature of these inclusions have been made.^{3–11} In order to confine solid noble gases at room temperature, the pressure must exceed 1–2 GPa. In metals, the structure of the noble-gas inclusions has been found to be fcc in a fcc matrix and hcp in a hcp matrix. The crystallites are often found, despite the sometimes very large lattice mismatch, to be epitactic with the matrix lattice.

This paper reports on solid noble-gas inclusions in a ceramic matrix. Ion implantation of ceramic materials has been investigated as a means of improving the hardness and wear of such materials.¹² The majority of previous studies have considered the implantation of Al_2O_3 with transition-metal ions (see, e.g., Ref. 13). Implantation using noble-gas ions is of interest in studying some of the fundamental aspects of the ion-implantation process as these ions are immiscible with the matrix and therefore chemical effects of ion implantation such as intermixing are unlikely.

In this study, transmission electron microscopy (TEM) has been used to examine the effects of ion implantation. TEM is a powerful technique for the examination of microstructure on a nanometer scale. A problem often encountered when conventional methods of specimen preparation for TEM analysis are used is the fact that the argon ion beam used to thin the ceramic may itself induce damage, which could be confused with the damage produced by intentional ion implantation. In the present TEM study, damage resulting from ion milling is entirely avoided by the use of a specimen preparation technique for the study of thin film or near-surface effects in ceramic materials.¹⁴ Ion implantation is performed directly into specially prepared electron-transparent thin-foil substrates, which can then be examined immediately following implantation. The method of preparation of such samples has been described in detail elsewhere.¹⁵ Im-

plantation of xenon ions was performed at room temperature using an accelerating voltage of 200 keV, to a projected range of ~ 50 nm. The ion fluence was varied from 1×10^{14} ions/cm² up to 2×10^{17} ions/cm².

Xenon was detected in samples implanted at fluences greater than 2×10^{15} ions/cm² by the use of energy-dispersive x-ray spectroscopy in the TEM. The physical state of the xenon was determined by analysis of selected-area diffraction (SAD) patterns. SAD patterns formed using a normal exposure time (to obtain the sharpest matrix reflections) did not reveal any additional reflections that could not be assigned to MgO. By forming SAD patterns using a much longer exposure time additional information could be obtained. Figure 1 shows a SAD pattern recorded from a sample implanted at a fluence of 5×10^{16} ions/cm². The (020), (220), and (111) reflections arising from MgO have been indexed and additional reflections are indicated by *A* and *B* in Fig. 1. These additional reflections were not observed in the SAD patterns recorded from unimplanted specimens or from specimens implanted at lower ion fluences. The reflections of the type labeled *A* are aligned with the (200) MgO reflections and are consistent with the lattice parameter of solid xenon. A diffuse ring *B* is also observed in diffraction patterns recorded from samples implanted at this level of fluence. Two possible explanations have been proposed to explain the formation of this ring pattern, which has also been observed in SAD patterns recorded from metals implanted with xenon. The ring may be due to diffraction from small xenon clusters which are randomly oriented with a respect to each other, i.e., they give a Debye-Scherrer ring.⁷ An alternative description has been proposed in which the ring formation is a result of xenon particles undergoing a solid-fluid phase transformation.¹⁰

Figure 2(a) is a bright-field image of a MgO thin-foil specimen implanted at a fluence of 2×10^{17} ions/cm². Roughly circular features, for example, area *A* in Fig. 2(a), are visible in the image; these features are up to 50 nm in diameter. A dark-field image formed using part of

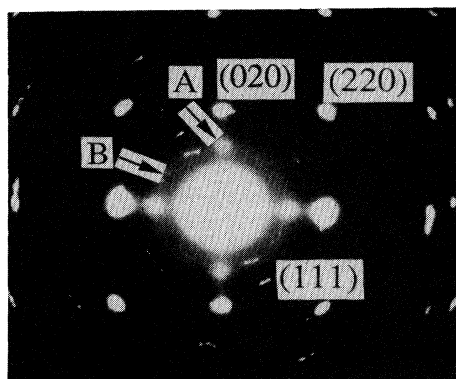


FIG. 1. Selected-area diffraction pattern recorded from a MgO specimen implanted with xenon at a fluence of 5×10^{16} ions/cm². The (020), (220), and (111) reflections from the MgO have been identified. Additional reflections due to the xenon inclusions are labeled *A* and *B*, the significance of these reflections is discussed in the text.

the ring pattern is shown in Fig. 2(b). From such images a distribution in the size of the particles can be determined. The larger particles, for example, *A* in Fig. 2(b), correspond to the features shown in Fig. 2(a). There are also a number of much smaller particles, for example, *B* in Fig. 2(b), having a diameter ~ 10 nm. From both the bright-field and dark-field images it can be seen that the xenon inclusions are uniformly distributed.

The fact that solid noble-gas inclusions have been detected by SAD at room temperature implies that they must be under a high pressure. The equilibrium pressure of an approximately spherical inclusion in a matrix is given by

$$P_{\text{eq}} = 2\gamma / r, \quad (1)$$

where γ is the interface energy per unit area and r is the radius of the particle. For noble-gas inclusions in metals the interface energy of the gas inclusions can be given by the surface energy of the matrix.¹⁶ For MgO a reasonable estimate of the surface energy is 1 J/m^2 ,¹⁷ so that the pressure of the large inclusions can be estimated to be ~ 0.1 GPa. For the smaller inclusions this pressure is ~ 0.4 GPa. An alternative method for calculation of the pressure, which does not rely on an estimated value of the surface energy, is to use a calculated value of the lattice parameter of the solid xenon from the diffraction pattern and then to use this value, 0.602 nm , in the Birch-Murnaghan equation of state:¹⁸

$$P = \frac{3}{2} B_0 [(V_0/V)^{7/3} - (V_0/V)^{5/3}] \times \left\{ 1 + \frac{3}{4} (B'_0 - 4) [(V_0/V)^{2/3} - 1] \right\}. \quad (2)$$

The following parameters were adopted in the calculation: the zero-pressure volume (V_0) used was $34.74 \text{ cm}^3/\text{mol}$,¹⁸ the molar volume (V) of the xenon was calculated to be $32.85 \text{ cm}^3/\text{mol}$, the values for the initial bulk modulus (B_0) and its pressure derivative (B'_0) were 10.17 and 4.0 GPa, respectively.¹⁹ This calculation gives a

value of the pressure for the solid particles as 0.63 GPa. This value is close to, but somewhat higher than, the value calculated for the small particles, using Eq. (1). The calculated pressure for the solid xenon inclusions in MgO is lower than that calculated for solid Xe and Kr inclusions in metals.^{20,21} This is due to the larger diameter of the particles found in this study. The reason for the differences in the particle size may in part derive from the fact that the bonding in a ceramic and metal matrix is different. However, it has been found in metal matrices that the shear modulus of the metal has a contributing factor on the gas pressure²² and this could be considerably larger for MgO (the shear modulus for Ni and MgO is ~ 79 and ~ 103 GPa, respectively). For metals, it appears that there is a limiting size effect for the formation of solid noble-gas inclusions. For Kr inclusions they are solid at room temperature to a maximum size of ~ 5 nm;⁸ this corresponds to a pressure of ~ 2 GPa. For Xe bubbles in Al they were found to be fluid at diameters

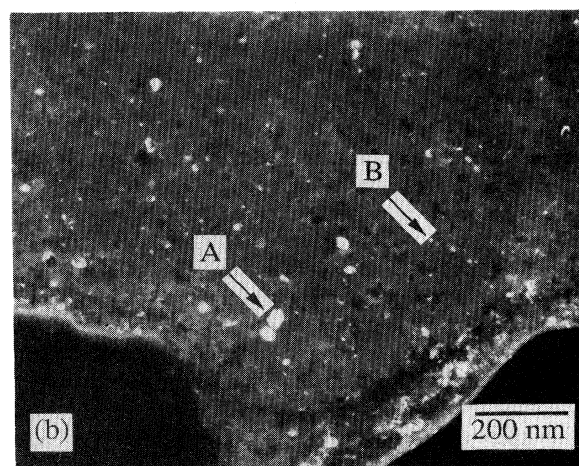
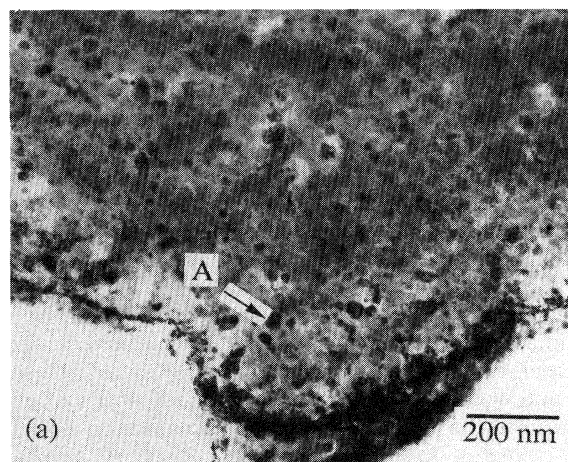


FIG. 2. (a) Bright-field image of a MgO thin-foil implanted at a fluence of 2×10^{17} ions/cm². Area *A* indicates a feature which has been attributed to a fluid xenon inclusion. (b) A dark-field image of the same area of the specimen shown in (a). The area labeled *A* is the same as that in (a). The small particles, e.g., *B*, are solid crystalline xenon inclusions.

~ 25 nm.¹⁰ However, pressure-temperature studies for bulk solid xenon have shown that at 300 K a pressure of 0.4 GPa is sufficient to maintain the solid phase. The small particles are thus solid, as demonstrated by the diffraction pattern, which shows clearly defined reflections which are consistent with the lattice parameter of solid xenon. However, the larger particles, where the pressure has been calculated to be ~ 0.1 GPa, are most likely fluid. This observation suggests that the ring pattern observed in the diffraction pattern may indeed, in part, be due to weak diffraction from fluid precipitates, although reflections due to misoriented solid material are visible within the ring itself.

The lattice parameters of face-centered cubic MgO and Xe (obtained from the Joint Committee for Powder Diffraction Standard powder diffraction files) are 0.421 and 0.626 nm, respectively. The unconstrained lattice misfit (δ) can be calculated from relationship (3) to give a value of $\sim 49\%$:

$$\delta = (a_{\text{Xe}} - a_{\text{MgO}}) / a_{\text{MgO}}, \quad (3)$$

where a_{Xe} and a_{MgO} are the lattice parameters of Xe and MgO, respectively. However, the lattice parameter of xenon determined from the diffraction pattern is smaller, 0.602 nm, thus a closer estimate of the lattice mismatch is $\sim 43\%$. The lattice parameter value for Xe is for the cubic structure, as it would be expected from studies in metals, that Xe would be cubic in the cubic MgO lattice. With such a large lattice mismatch it would be expected that the interface between the crystalline xenon inclusions and the matrix would be incoherent. This result might be inferred by the roughly spherical shape of the inclusions. It is still possible, however, for the interface to be incoherent and for the faceting of the inclusions to occur. Such faceting has been seen for solid Kr inclusions in Ni.²³ The value of the xenon lattice parameter calculated from xenon ion implantation in metals (see, e.g., Ref. 20) is smaller than that found in this present study. The difference is due to the generally larger pressures and smaller size of the solid gas inclusions in the metal matrix. Therefore it can be seen that the lattice parameter is a function of the pressure, and that as the pressure increases the lattice parameter, and therefore the lattice mismatch, decreases. It might also be expected that

the interface energy will actually depend on the pressure in the particle through its influence on a_{Xe} . Further studies of the precipitate-matrix interface are in progress using high-resolution electron microscopy.

It is interesting to consider the possible effect, if any, of these inclusions on the mechanical properties of MgO following implantation. The implanted material represents a two-phase material and often hardness increases are obtained by formation of a two-phase microstructure as in the case of ZrO₂-toughened Al₂O₃ or other composite ceramic materials. The bulk modulus of solid xenon is low¹⁹ and therefore it will easily be deformed under applied stress. Also, a propagating crack impinging on a xenon inclusion will release the matrix constraint on the inclusion. The solid will then vaporize, resulting in a two-phase material where the second phase is a void. This situation represents the limiting case for a two-phase material, where one phase has zero stiffness. It differs from other composites in that the elastic properties of the "inclusion" phase drastically change when a crack actually penetrates the "particle." An important consideration will also be the nature of the precipitate-matrix interface, as it is this interface that often controls the nature of crack propagation.

In conclusion, xenon inclusions in a MgO matrix have been detected following ion implantation. These inclusions range from 10 to 50 nm in diameter. The small particles have been determined to be solid at room temperature. The presence of a solid noble gas at room temperature necessitates that they are under a high pressure, which, in the situation described here, has been calculated to be 0.4–0.6 GPa. The pressure of the larger particles is ~ 0.1 GPa, indicating that they are almost certainly fluid at room temperature. A proportion of the solid particles are epitaxial with the matrix as determined by an examination of the SAD patterns.

This research has been supported by the National Science Foundation (through use of the National Nanofabrication Facility and the Materials Science Center), Corning Incorporated, and the Army Research Organization. One of us (M.G.N.) was supported by the Materials Science Center at Cornell. The authors are grateful to Professor Y. K. Vohra for his valuable comments on this research.

¹A. vomFelde, J. Fink, Th. Muller-Heinzerling, J. Pfluger, B. Scheerer, G. Linker, and D. Kaletta, *Phys. Rev. Lett.* **53**, 922 (1984).

²C. Templier, C. Jaoueu, J. P. Riviere, J. Delafond, and J. Grilhe, *C. R. Acad. Sci. Ser.* **299**, 613 (1984).

³J. H. Evans and D. J. Mazey, *Scr. Metall.* **19**, 621 (1985).

⁴R. C. Birtcher and W. Jager, *J. Nucl. Mater.* **135**, 274 (1985).

⁵C. Templier, R. J. Gaboriand, and H. Garem, *Mater. Sci. Eng.* **69**, 63 (1985).

⁶J. H. Evans and D. J. Mazey, *J. Phys. F* **15**, L1 (1985).

⁷C. Templier, H. Garem, and J. P. Riviere, *Philos. Mag. A* **53**, 667 (1986).

⁸R. C. Birtcher and W. Jager, *Ultramicroscopy* **22**, 267 (1987).

⁹J. H. Evans and D. J. Mazey, *J. Nucl. Mater.* **138**, 176 (1986).

¹⁰J. C. Desoyer, C. Templier, J. Delafond, and H. Garem, *Nucl. Instrum. Methods Phys. Res. B* **19/20**, 450 (1987).

¹¹H. H. Anderson, J. Bohr, A. Johansen, E. Johnson, L. Sarholt-Kristensen, and V. Surganov, *Phys. Rev. Lett.* **59**, 1589 (1987).

¹²P. J. Burnett and T. F. Page, *Radiat. Eff.* **97**, 123 (1986).

¹³C. W. White, C. J. McHargue, P. S. Sklad, L. A. Boatner, and G. C. Farlow, *Mater. Sci. Rep.* **4**, 41 (1989).

¹⁴C. B. Carter, S. R. Summerfelt, L. A. Tietz, M. G. Norton, and D. W. Susnitzky, in *EMAG MICRO 89*, Proceedings of the Electron Microscopy and Analysis Group and Royal Microscopical Society Conference, edited by P. J. Goodhew and

- H. Y. Elder, IOP Conf. Proc. No. 98 (Institute of Physics and Physical Society, London, 1989), p. 415.
- ¹⁵M. G. Norton, S. R. Summerfelt, and C. B. Carter, Appl. Phys. Lett. **56**, 2246 (1990).
- ¹⁶A. R. Miedema, Solid State Commun. **39**, 1337 (1981).
- ¹⁷W. D. Kingery, H. K. Bowen, and D. R. Uhlmann, *Introduction to Ceramics*, 2nd ed. (Wiley, New York, 1975).
- ¹⁸K. Asaumi, Phys. Rev. B **29**, 7026 (1984).
- ¹⁹R. Reichlin, K. E. Brister, A. K. McMahan, M. Ross, S. Martin, Y. K. Vohra, and A. L. Ruoff, Phys. Rev. Lett. **62**, 669 (1989).
- ²⁰C. Templier, H. Garem, J. P. Riviere, and J. Delafond, Nucl. Instrum. Methods Phys. Res. B **18**, 24 (1986).
- ²¹L. Grabaek, J. Bohr, E. Johnson, H. H. Anderson, A. Johansen, and L. Sarholt-Kristensen, Mater. Sci. Eng. A **115**, 97 (1989).
- ²²J. H. Evans, in *Fundamentals of Beam-Solid Interactions and Transient Thermal Processing*, edited by M. J. Aziz, L. E. Rehn, and B. Stritzker, MRS Symposia Proceedings No. 100 (Materials Research Society, Pittsburgh, 1988), p. 219.
- ²³R. C. Bircher and A. S. Liu, in *Fundamentals of Beam-Solid Interactions and Transient Thermal Processing* (Ref. 22), p. 225.

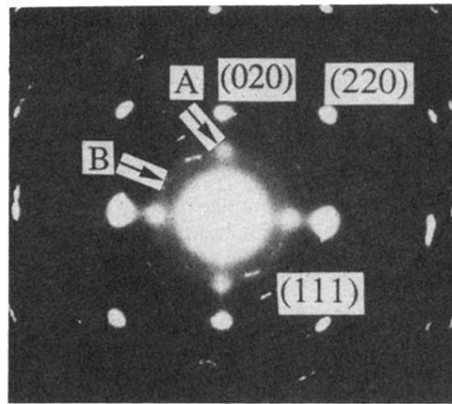


FIG. 1. Selected-area diffraction pattern recorded from a MgO specimen implanted with xenon at a fluence of 5×10^{16} ions/cm². The (020), (220), and (111) reflections from the MgO have been identified. Additional reflections due to the xenon inclusions are labeled *A* and *B*, the significance of these reflections is discussed in the text.

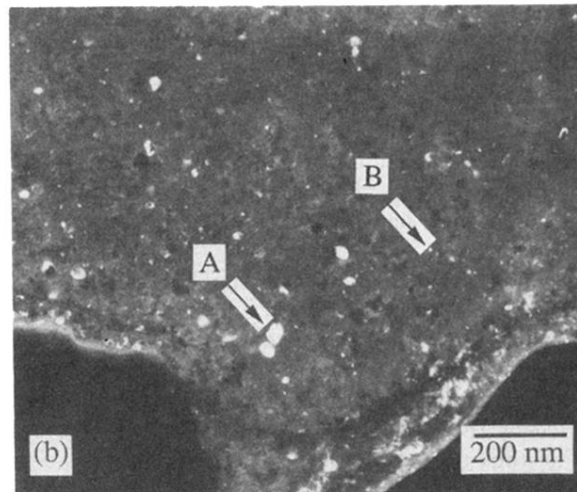
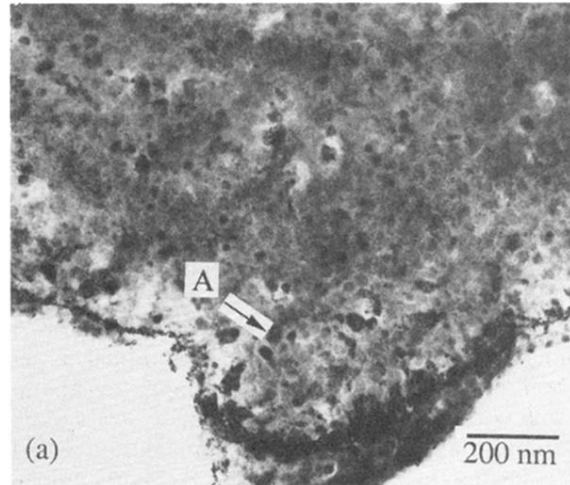


FIG. 2. (a) Bright-field image of a MgO thin-foil implanted at a fluence of 2×10^{17} ions/cm². Area *A* indicates a feature which has been attributed to a fluid xenon inclusion. (b) A dark-field image of the same area of the specimen shown in (a). The area labeled *A* is the same as that in (a). The small particles, e.g., *B*, are solid crystalline xenon inclusions.